Broad-Band Operation of Stripline *Y* Circulators

TSUKASA NAGAO, MEMBER, IEEE

Abstract—**The broad-band operation of stripline *Y* circulators is treated from the viewpoint of the double circulation frequency operation (DCFO) which is performed with conductor-dielectric-ferrite composites (CDF composites), without any broad-banding circuit externally connected. It is recognized that the conductive post inserted inside the dielectric-ferrite composite (DF composite—a CDF composite is made thereby) is effective to improve the isolation characteristics of a CDF composite circulator to achieve the broad-band operation. The experiments showed that the frequency band was continuously broad-banded by sequentially changing the biasing magnetic field intensity; whereupon the frequency band reached about 45 percent. The largest broad-band operation was obtained when four circulation frequencies were put into use. In this paper, all ferrites are biased magnetically above resonance.**

I. Introduction

THE BROAD-BANDING of stripline *Y* circulators has long received much attention in devices using disk ferrites. Fay and Comstock [1] demonstrated a method to obtain broad-band circulators by using a quarter wavelength transformer for impedance matching. Many people have also demonstrated the utility of broad-banding transformers [2]–[4]. Recently, Wu and Rosenbaum have succeeded in realizing wide-band operation of a microstrip *Y* circulator, using only microstrip tapers [5]. It stems from the fact that there is a wide-band condition, with respect to the lowest order circulation (mode 1), in the course of the circulation adjustments.

One can say all the aforementioned circulators belong to the operation of only mode 1, according to the labeling given by Davies and Cohen [6]. Very recently, the author has reported on DCFO [7], which was performed with DF composites. The broad-band operation which will be discussed is, in principle, an application of DCFO. A circulator with a DCFO can operate at dual circulation frequencies, but cannot operate between them because the perfect circulation condition is not wholly satisfied in an intercirculation frequency region. The DCFO performance is evidently marked by less isolation than the 20-dB level in the intercirculation frequency. However, if the performance characteristics in the intercirculation frequency are improved, the broad-banding is consequently realized. Broad-band operation in this manner has been obtained in the *Y*-junction with CDF composites as shown in Fig. 1. The utility of a conductive post inserted inside a closely fitting ferrite has been discussed in [8]–[10], but its effect in the presence of dielectric between the conductive post and the ferrite is not treated yet, as far as the author is aware.

In this paper, computed results of perfect circulation conditions are presented and the effect of a conductive post inside the composite is examined. Theoretical performances are discussed in comparison with experimental results. Circulator performances and identification of circulation modes are also demonstrated. All treatments are made above resonance.

Manuscript received May 12, 1977; revised July 20, 1977.

The author is with the Department of Electrical Engineering, National Defense Academy, Hashirimizu, Yokosuka, Kanagawa 239, Japan.

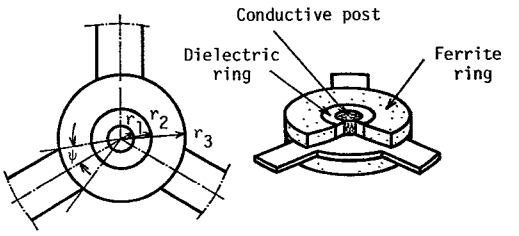

Fig. 1. (a) Configurations of stripline *Y*-junction. (b) CDF composites used therein.

II. Theoretical Treatment

A. Electromagnetic (EM) Fields in the CDF Composite

It is assumed that in the EM fields the electric field has only the z-component and that the EM fields are independent of the z-coordinate in the cylindrical coordinate (r,θ,z). Using the null condition of the tangential electric field on the conductive post, and applying the continuity conditions between tangential magnetic field components in the dielectric and the ferrite rings at their boundary $r = r_2$, one can obtain the following EM fields in the ferrite ring $(r_2 < r < r_3)$:

$$E_z = \sum_{n=-\infty}^{\infty} a_n F_n(x) e^{-jn\theta} \tag{1}$$

$$H_r = -j\left[\frac{1}{r}\frac{\partial E_z}{\partial \theta} + j\frac{\kappa}{\mu}\frac{\partial E_z}{\partial r}\right] \Big/ \omega\mu_0\mu_e$$

$$H_\theta = j\left[\frac{\partial E_z}{\partial r} - j\frac{\kappa}{\mu}\frac{1}{r}\frac{\partial E_z}{\partial \theta}\right] \Big/ \omega\mu_0\mu_e \tag{2}$$

where

$$F_n(x) = J_n(x) + C_n Y_n(x)$$

$$F_n'(x) = J_n'(x) + C_n Y_n'(x)$$

$$C_n = -[J_n'(x_3) - J_n(x_3)I_n]/[Y_n'(x_3) - Y_n(x_3)I_n]$$

$$I_n = \frac{\zeta_2}{\zeta_1}\frac{J_n'(x_2) + D_n Y_n'(x_2)}{J_n(x_2) + D_n Y_n(x_2)} + \frac{\kappa}{\mu}\frac{n}{x_3}$$

$$D_n = -\frac{J_n(x_1)}{Y_n(x_1)}$$

$$x = k_2 r \le x_4, \qquad x_4 = k_2 r_3, \qquad x_3 = k_2 r_2,$$

$$x_2 = k_1 r_2, \qquad x_1 = k_1 r_1 \tag{3}$$

and

J_n, Y_n Bessel functions of the first and second kinds, respectively, and "′" denotes their derivatives;

k_1, k_2 $k_1 = \omega\sqrt{\varepsilon_0 \varepsilon_1 \mu_0}$ and $k_2 = \omega\sqrt{\varepsilon_0 \varepsilon_2 \mu_0 \mu_e}$, radial wave propagation constants in the dielectric and the ferrite, respectively;

ζ_1, ζ_2 $\zeta_1 = \sqrt{\mu_0/\varepsilon_0 \varepsilon_1}$ and $\zeta_2 = \sqrt{\mu_0 \mu_e/\varepsilon_0 \varepsilon_2}$, intrinsic wave impedances of the dielectric and the ferrite, respectively;

ε_1 specific permittivity of the dielectric ring;

ε_2, μ_e specific permittivity and effective permeability of the ferrite and $\mu_e = \mu[1 - (\kappa/\mu)^2]$;

κ, μ elements of ferrite permeability tensor;

r_1, r_2, r_3 outer radii of conductive post, dielectric and ferrite rings, respectively.

One can construct the so-called Bosma's Green's function to analyze the circulator action of the Y-junction with the CDF composites, using the EM fields. To get rid of some tedius manipulations in theoretical treatments, the two circulation condition equations given in [7] are used.

B. Resonance Curves, the First and the Second Circulation Condition Curves

The resonant modes are defined by applying the condition of a magnetically short-circuited edge at the periphery of the composite to the tangential magnetic field of (2). One can obtain the following equations:

$$F_n'(x_4) - \frac{\kappa}{\mu}\frac{n}{x_4} F_n(x_4) = 0, \qquad n = 0, \pm 1, \pm 2, \cdots. \quad (4)$$

Computed results of (4) are shown in Fig. 2(a).

Computation of the first and the second circulation conditions is made as follows. Let us first rewrite the two conditional equations

$$(h_0 + h_1 + h_2)(h_0 h_1 + h_1 h_2 + h_2 h_0) - 9 h_0 h_1 h_2 = 0 \quad (5)$$

$$\frac{\psi}{\pi}(\zeta_2/\zeta_d) = (h_1 - h_2)/[2h_1 h_2 - h_0(h_1 + h_2)] \quad (6)$$

where these quantities h_0, h_1, and h_2 are defined by

$$h_0 = \sum_{m=0}^{\infty} S(3m\psi) 2 f_{3ma}/[f_{3ma}^2 - (g_{3m} - f_{3ms})^2]$$

$$h_1 = \sum_{m=-\infty}^{\infty} S[(3m+1)\psi]/[f_{3m+1} - g_{3m+1}]$$

$$h_2 = \sum_{m=-\infty}^{\infty} S[(3m-1)\psi]/[f_{3m-1} - g_{3m-1}] \quad (7)$$

and, for all $n = 3m - 1$, $3m$, and $3m + 1$

$$f_n = F_n'(x_4)/F_n(x_4)$$

$$g_n = \frac{\kappa}{\mu}\frac{n}{x_4}$$

$$S(n\psi) = \sin(n\psi)/n\psi$$

$$f_{na} = (f_n + f_{-n})/2$$

$$f_{ns} = (f_n - f_{-n})/2. \quad (8)$$

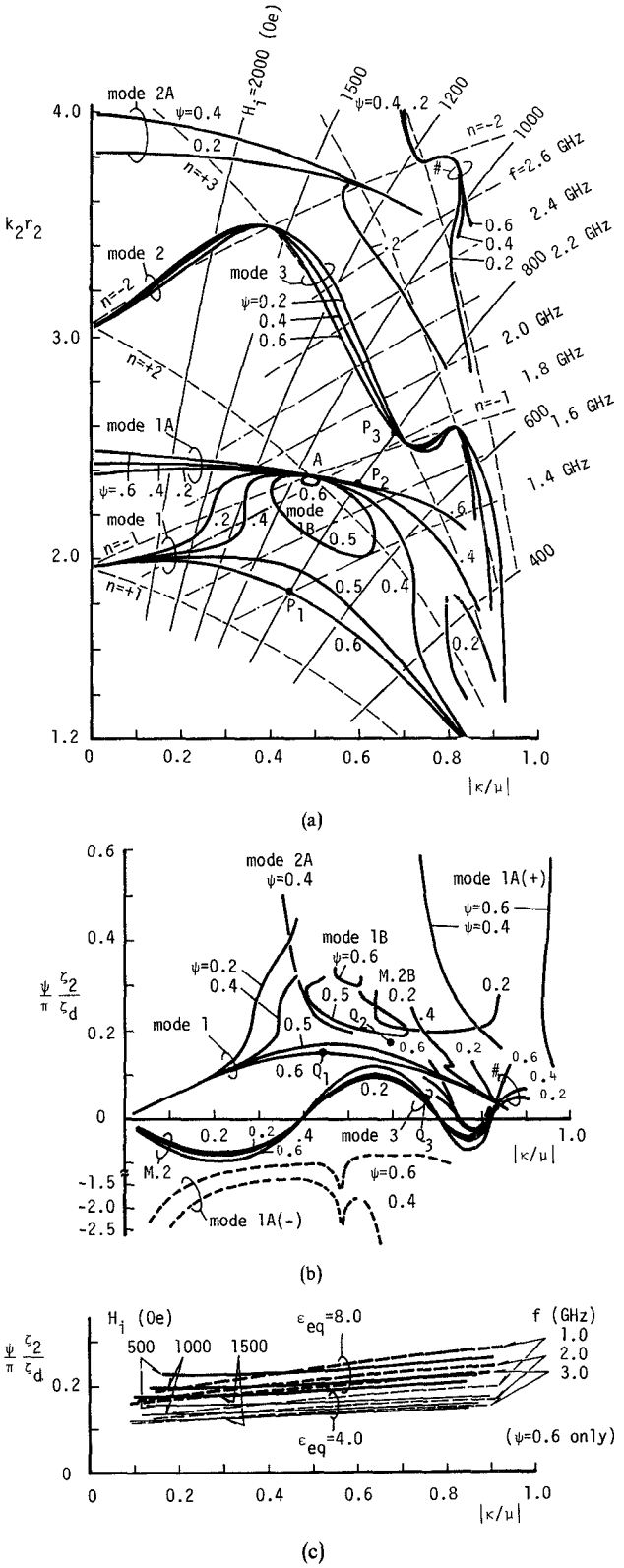

Fig. 2. Computed results of the first and the second circulation conditions. (a) The first circulation condition curves, where broken thin lines (----) show resonant mode curves of uncoupled ($\psi = 0$) CDF composite resonator (the + and − signs denote clockwise and counterclockwise rotating modes, respectively), thin lines (———) show loci of constant internal magnetic field intensity, and thin dot-dashed lines (—·—·—) show loci of constant frequency. ψ is half the coupling angle subtending the stripline at the center conductor. (b) The computed results of the right term of the second conditional equation (6). (c) The computed results of the left term of (6), for $\psi = 0.6$.

ψ is half the coupling angle subtending the stripline width at the junction.

Computation of (5) and the right term of (6) is made by retaining terms up to $n = 6$ and by using Polder's equations of permeability tensor [11]. Computed results are shown in Fig. 2(a) and (b). They are functions of radius ratios r_1/r_3 and r_2/r_3, wave propagation constant ratio k_1/k_2, and intrinsic wave impedance ratio ζ_1/ζ_2. These parameters are chosen in accordance with the actual geometry of the circulator used in the experiments given later. They are that $r_1/r_3 = 0.15$, $r_2/r_3 = 0.3$, and $r_3 = 10$ mm; and the saturation magnetization of the ferrite $4\pi M_s = 1200$ G, $\varepsilon_2 = 14.5$, and $\varepsilon_1 = 1$.

Computation of the left term of (6) is made using the relation

$$\zeta_2/\zeta_d = \sqrt{\varepsilon_{eq}\mu_e/\varepsilon_2} \tag{9}$$

where ε_{eq} is an equivalent permittivity assumed to include all the factors depending on the geometry of stripline and dielectric pervaded therein. ε_{eq} differs from a specific permittivity of dielectric actually used and it gives a large value of ζ_d when ε_{eq} is small. However, it provides the relationship of constant internal magnetic field and frequency. Computed results of the left term of (6) is shown in Fig. 2(c), for $\psi = 0.6$ only.

General features of the first circulation condition curves are similar to those of a DF composite circulator [7] or a disk ferrite circulator [6], [12], but the mode 1 curves conspicuously present a contrast. The mode 1 curves converge to the degenerate point $k_2 r_3 \simeq 1.96$, $\kappa/\mu = 0$, which is higher than the point $k_0 r_0 \simeq 1.84$ for a disk ferrite circulator. The $k_2 r_3$ value at the degenerate point for mode 1 increases as the ratio r_2/r_3 of the CDF composite as well as a DF composite [7], in that the magnetic field energy stored in the ferrite portion for each of rotating resonant modes is reduced as the ratio r_2/r_3 increases.

It is remarked that the tightly coupled circulation holds for $\psi \geq 0.5$ since the first circulation roots of mode 1 go down with increasing κ/μ, and the lightly coupled circulation for $\psi < 0.5$. For $0.5 < \psi < 0.6$, the first circulation roots split into mode 1 and mode 1B, and for $\psi \gg 0.6$, mode 1B disappears. Meanwhile, in the case of the DF composite circulator [7], it is tightly coupled for $\psi \geq 0.7$. This is to be caused by the conductive post inside the CDF composite.

Computed results of the right term of (6), as shown in Fig. 2(b), also make a sharp contrast with those of the DF composite circulator [7]. The mode 1 curves, for $0.5 < \psi < 0.6$ and $0.3 < \kappa/\mu < 0.6$, flatly run holding the value of $(\psi/\pi)(\zeta_2/\zeta_d)$ which is nearly equal to 0.2, as well as modes 1B, 2A, and 2B, but mode 3 holds a slightly low value of $(\psi/\pi)(\zeta_2/\zeta_d)$ even at its maximum for $\kappa/\mu \simeq 0.5$. These conditions are desirable for adjustment of the second circulation condition in the intercirculation frequency, because such condition curves can coincide over a wide range with a locus of constant internal magnetic field in the second circulation condition, as shown in Fig. 2(c).

Operating points are determined by intersections of the first condition curves and a locus of internal magnetic field H_i and specified by sets of κ/μ, H_i, and frequency. For instance, see points P_1, P_2, and P_3. The second condition must be satisfied at these points to get perfect circulation. This is achieved in such a graphic way that corresponding points Q_1, Q_2, and Q_3, having the same sets of specific values determined in the first condition curves, are found on respective mode curves in the second condition curves of the right term of (6), as shown in Fig. 2(b); and next they are adjusted to coincide with one locus of the same internal magnetic field H_i in the second condition curves of the left term of (6), as shown in Fig. 2(c). Such circulation adjustments can be performed when two operating points of modes 1 and 1A(+), for instance, are selected for $0.5 < \psi < 0.6$, in that these modes can hold similarly large values of $(\psi/\pi)(\zeta_2/\zeta_d)$.

It is remarked that mode 1A holds the large and negative value of $(\psi/\pi)(\zeta_2/\zeta_d)$ for $(\kappa/\mu) \leq 0.6$ and $\psi = 0.4$, and for $(\kappa/\mu) \leq 0.8$ and $\psi = 0.6$, which is denoted by mode 1A(−) against mode 1A(+). This state of mode 1A does not support the possibility of a DCFO with mode 1 in a higher internal magnetic field than $H_i = 700$ Oe. Multiple circulations with so many operating points can be discussed likewise.

C. Theoretical Performances and Input Impedances

To examine the effect of impedance matching by use of the conductive post, computation is made of the input impedance of the Y-junction and its circulator performance for various ratios of r_1/r_3, under the constant dimension of the composite.

As a start, the input impedance of the Y-junction is derived. Since the junction mode impedances are given by

$$Z^{(0)} = j\sqrt{3}\frac{\psi}{\pi}\zeta_2 h_0$$

$$Z^{(+1)} = j\sqrt{3}\frac{\psi}{\pi}\zeta_2 h_1$$

$$Z^{(-1)} = j\sqrt{3}\frac{\psi}{\pi}\zeta_2 h_2 \tag{10}$$

substituting them into the following relations for elements of the impedance matrix representing the Y-junction

$$Z_1 = \tfrac{1}{3}[Z^{(0)} + Z^{(+1)} + Z^{(-1)}]$$

$$Z_2 = \tfrac{1}{3}[Z^{(0)} + Z^{(+1)}\omega + Z^{(-1)}\omega^2]$$

$$Z_3 = \tfrac{1}{3}[Z^{(0)} + Z^{(+1)}\omega^2 + Z^{(-1)}\omega], \quad \omega = \exp(j\tfrac{2}{3}\pi) \tag{11}$$

one can derive the input impedance normalized by the wave impedance ζ_d of the coupled stripline

$$\bar{Z}_{in} = -1 - Z_0/[\zeta_d\{Z_2 Z_3 - (\zeta_d + Z_1)^2\}] \tag{12}$$

where

$$Z_0 = (\zeta_d + Z^{(0)})(\zeta_d + Z^{(+1)})(\zeta_d + Z^{(-1)}).$$

The circulator characteristics are specified by return loss, isolation, and insertion loss, which are defined by

$$\text{return loss} \quad = 20 \log_{10} \alpha \tag{13}$$

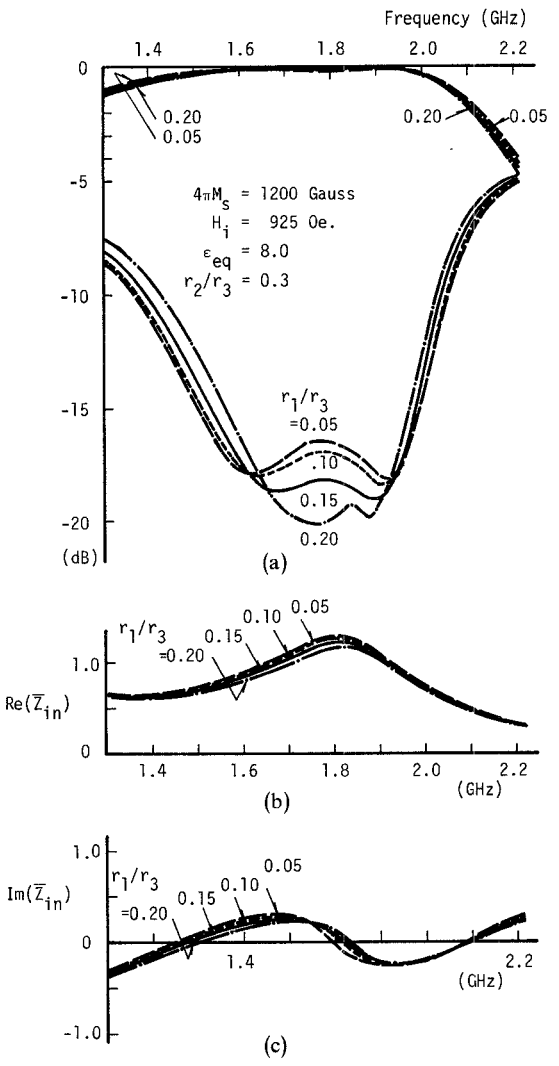

Fig. 3. (a) Theoretical performances and normalized input impedances for various ratios of r_1/r_3 of the conductive post. Real and imaginary parts of the normalized input impedance are denoted by (b) Re $(\bar{Z}_{in})$ and (c) Im $(\bar{Z}_{in})$, respectively.

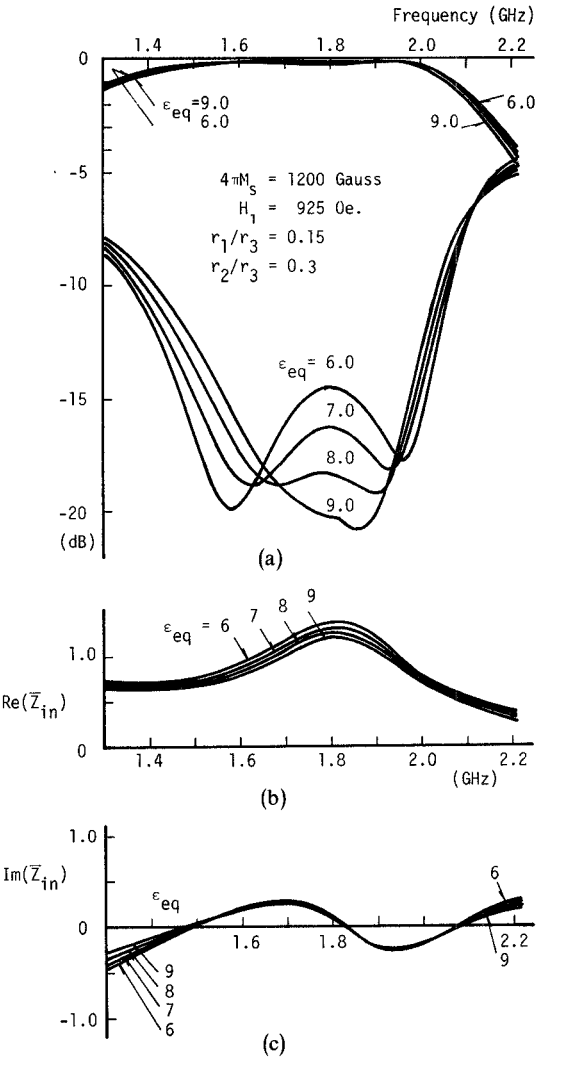

Fig. 4. (a) Theoretical performances and normalized input impedances for various values of ε_{eq}, an equivalent permittivity. Real and imaginary parts of the normalized input impedance are denoted by (b) Re $(\bar{Z}_{in})$ and (c) Im $(\bar{Z}_{in})$, respectively.

$$\text{insertion loss} = 20 \log_{10} \beta \tag{14}$$

$$\text{isolation} = 20 \log_{10} \gamma. \tag{15}$$

α, β, and γ are scattering matrix elements of the Y-junction given by

$$\alpha = 1 + 2\{Z_2 Z_3 - (\zeta_d + Z_1)^2\}\zeta_d / Z_0 \tag{16}$$

$$\beta = 2\{Z_3(\zeta_d + Z_1) - Z_2^2\}\zeta_d / Z_0 \tag{17}$$

$$\gamma = 2\{(\zeta_d + Z_1)Z_2 - Z_3^2\}\zeta_d / Z_0. \tag{18}$$

Only one case for DCFO is cited. A primary concern is to investigate the effect of a conductive post on isolation in the intercirculation frequency region. Necessary parameters are determined from circulation frequencies of the DCFO measured in the experiments as will be seen in Fig. 5(a). Other specifications of the circulator used are taken into account. The wave impedance ζ_d of the stripline is approximated by $\sqrt{\mu_0/\varepsilon_0 \varepsilon_{eq}}$.

Computation of (12), (14), and (15) is made, retaining terms up to $n = 9$, along with the locus of constant internal magnetic field $H_i = 925$ Oe. The essential difference is that the computation is made with modes 1 and 3, whereas the experiment as shown in Fig. 5(a) was done with modes 1 and 1A. This is done because there is no pair of operating points of modes 1 and 1A to hold such circulation frequencies of the cited DCFO experiment. Alternatively, the pair of modes 1 and 3 is taken for theoretical analysis, and $\psi = 0.6$ for the tightly coupled circulation is chosen so as to meet the second condition, because the conductive post does not selectively favor the DCFO with modes 1 and 3, or others.

The dependence on r_1/r_3 is demonstrated in Fig. 3. As for $r_1/r_3 = 0$, the composite is free from a conductive post and a DF composite. The theoretical performance typically shows a DCFO, and has the isolation lower than the 20 dB in the intercirculation frequency since the real part of $\bar{Z}_{in}$ is too high. As r_1/r_3 is increased, the theoretical performances demonstrate improvement of the isolation at the intercirculation frequency. It corresponds to lowering of the peak value of the real part of $\bar{Z}_{in}$. Generally, with having the

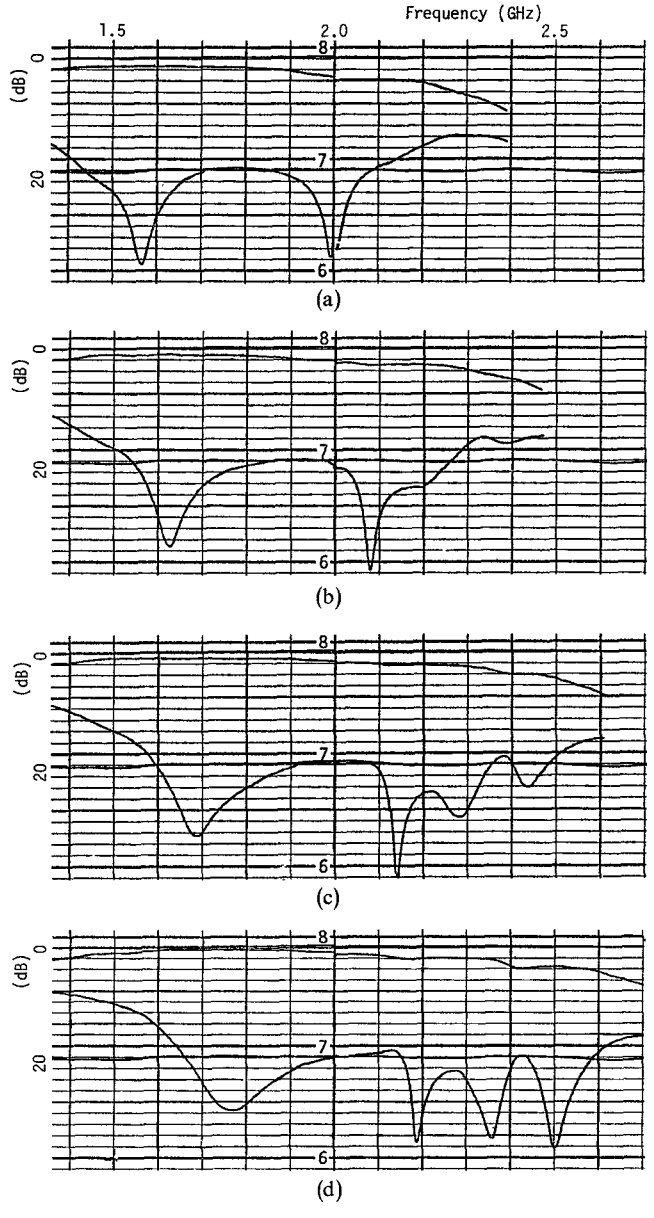

Fig. 5. Experimental examples of the broad-band operation with sequential change of the biasing magnetic field. Figs. 5(a), (b), (c), and (d), respectively, show the cases of the biasing magnetic fields $H_{ex} = 900$, 950, 1000, and 1050 Oe. The upper curve of each figure is insertion loss and the lower curve is isolation.

conductive post, the imaginary part of $\bar{Z}_{in}$ is also lowered to a minor degree.

Theoretical performances are shown in Fig. 4, for various values of ε_{eq}. Variation of ε_{eq} is effective in altering isolation characteristics through affecting the real part of $\bar{Z}_{in}$.

Thus impedance matching in the intercirculation frequency is effectively achieved by enlarging the conductive post to the ratio of $r_1/r_3 = 0.15$. A further enlarged post, however, does not bring forth any favorable effect because it alters the lightly coupled circulation to the tightly coupled case, and the second condition is no longer satisfied.

Needless to say, these performances merely account for the circulation characteristics at a certain point close to the junction connecting the center conductor with coupled

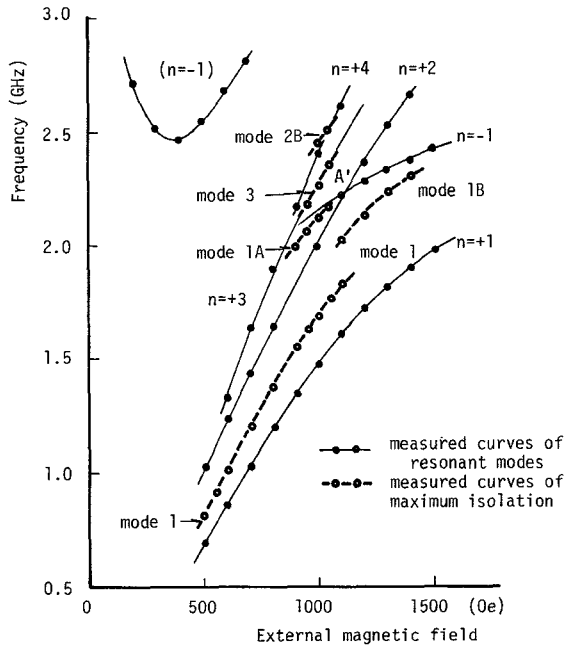

Fig. 6. Identification of circulation modes in the mode chart of the CDF composite resonator. A number in parentheses denotes the resonant mode below resonance.

stripline taper. Therefore, the final performance of the circulator action must be evaluated at the output of the coupled taper. Practically, through the tapers, the input impedance is matched to the 50-Ω transmission lines and the aforementioned theoretical performances are expected to be improved.

III. Experiments and Discussions

A. Experimental Examples

The experimental examples are demonstrated in Fig. 5. The composite used was made from a ferrite ring with the outer radius $r_3 = 10$ mm and the inner radius $r_2 = 3$ mm, and the conductive post with the radius $r_1 = 1.5$ mm. The ferrite material was Al–YIG, with the specifications that the saturation magnetization $4\pi M_s = 1200$ G, the half-width $\Delta H = 80$ Oe, and the specific permittivity $\varepsilon_2 = 14.5$. The stripline width was 11 mm, which corresponded to $\psi = 0.58$. Stripline tapers were used to connect the Y-junction to the external transmission lines.

Typical performances were obtained in sequential change of the biasing magnetic field around the field intensity $H_{ex} = 1000$ Oe. Circulator actions were featured by double to quadruple peaks of isolation, with the magnetic field increased. The insertion losses showed a tendency to increase slightly in the vicinity of the highest circulation frequency. The frequency band reached 45 percent when four circulation frequencies were put into use.

B. Discussions

To identify circulation modes, operating points measured from isolation peaks are plotted superimposed in the mode chart of the CDF composite resonator as shown in Fig. 6.

There is a curve of mode 1 in the region bounded by the resonance curves $n = +1, -1$, and $+2$. Mode 1A is in the region bounded by the resonance curves $n = -1$ and $+2$. Mode 3 is between the resonance curves $n = +2$ and $+4$, and mode 2B is coincidental with the resonance curve $n = +4$. The resonance curve $n = +3$ was not discernible. Location of these modes completely agrees with the first circulation condition curves as shown in Fig. 2(a). The curve of mode 1 shows a pattern of the tightly coupled circulation.

Broad-band operations can be described in terms of these circulation modes. Modes 1 and 1A play their respective roles in the DCFO under low-magnetic field, and accordingly, as the biasing magnetic field is increased, other higher order modes join those modes. The experiments showed that modes 1, 1A, 3, and 2B played distinct roles.

In comparing theoretical and experimental performances, and also the first circulation condition curves (Fig. 2(a)) and operating curves in the mode chart (Fig. 6), one can recognize some contrasts between them. First, there is no theoretical performance corresponding to a DCFO of 1.5 and 2.0 GHz for modes 1 and 1A, respectively, as shown in Fig. 5(a). Next, mode 1A did not change the circulating direction in lower biasing magnetic field than the intersection A', as shown in Fig. 6, while mode 1A changes its sign of $(\psi/\pi)(\zeta_2/\zeta_d)$ and hence the circulating direction as shown in Fig. 2(b). However, in the experiments, as shown in Fig. 5(d), four modes (1, 1A, 3, and 2B) played their roles. This particular condition seems to not completely fit to any locus of constant internal magnetic field in the first condition curves, as shown in Fig. 2(a), but it is found out that there is a like condition (except mode 1A) in a narrow region in the vicinity of and in lower internal magnetic field than the intersection A. The reason is probably that the resonant modal pattern in the real CDF composite is slightly different from the theoretically predicted pattern, because the cross section of the ring ferrite is not thin enough and hence internal magnetic field distribution is no longer uniform.

IV. Conclusions

The broad-band operation of the stripline Y circulator is performed by use of the CDF composite. It is, in principle, an application of DCFO. The DCFO performance normally shows less isolation than the 20-dB level in the intercirculation frequency. The broad-band operation is realized when such low isolation is improved. The conductive post in the CDF composite has the effect to lower the input impedance of the Y-junction and to achieve impedance matching. It, of course, changes the modal patterns of the DF composite and hence the resonant frequencies.

The circulator action with the CDF composites is theoretically treated, by making use of the perfect circulation conditions. Input impedance characteristics and theoretical performances, particularly regarding DCFO, are demonstrated.

Experiments of the broad-band operation are also presented. A broad-band operation with a DCFO was performed under a low magnetic field. When the biasing magnetic field was increased, large broad-band operations took place with many circulation frequencies. These operations are identified in the mode chart of the CDF composite resonator.

Comparisons between theoretical and experimental performances do not support complete agreement, and the discrepancies between them are considered to be caused by the internal magnetic field distribution inside the ferrite element of the composite.

The circulator of this broad-band operation has the performance advantage that it is compact, and easy to adjust, that it is unnecessary to use any broad-banding circuit externally connected for impedance matching, and that it can vary the frequency band continuously in accordance with the biasing magnetic field intensity.

Acknowledgment

The author wishes to thank Z. Tanaka for his cooperation, and S. Takata and K. Yokoyama of the TDK Electronics Company for their helpful discussions and support.

References

[1] C. E. Fay and R. L. Comstock, "Operation of the ferrite junction circulator," *IEEE Trans. Microwave Theory Tech.*, vol. MTT-13, pp. 15–27, Jan. 1965.

[2] J. W. Simon, "Broadband strip-transmission line Y-junction circulators," *IEEE Trans. Microwave Theory Tech.*, vol. MTT-13, pp. 335–345, May 1965.

[3] L. K. Anderson, "Analysis of broadband circulators with external tuning elements," *IEEE Trans. Microwave Theory Tech.*, vol. MTT-15, pp. 42–47, Jan. 1967.

[4] E. Schwartz, "Broadband matching of resonant circuits and circulators," *IEEE Trans. Microwave Theory Tech.*, vol. MTT-16, pp. 158–165, Mar. 1968.

[5] Y. S. Wu and F. J. Rosenbaum, "Wideband operation of microstrip circulators," *IEEE Trans. Microwave Theory Tech.*, vol. MTT-22, pp. 849–856, Oct. 1974.

[6] J. B. Davies and P. Cohen, "Theoretical design of symmetrical junction stripline circulator," *IEEE Trans. Microwave Theory Tech.*, vol. MTT-11, pp. 506–512, Nov. 1963.

[7] T. Nagao, "Double circulation frequency operation of stripline Y-junction circulators," *IEEE Trans. Microwave Theory Tech.*, vol. MTT-25, pp. 181–189, Mar. 1977.

[8] L. E. Davis, M. D Coleman, and J. J. Cotter, "Fourport crossed-waveguide junction circulators," *IEEE Trans. Microwave Theory Tech.*, vol. MTT-12, pp. 43–47, Jan. 1964.

[9] C. G. Parsonson, S. R. Longly, and J. B. Davies, "Theoretical design of broadband 3-port waveguide circulators," *IEEE Trans. Microwave Theory Tech.*, vol MTT-16, pp. 256–258, Apr. 1968.

[10] R. S. Mueller and F. J. Rosenbaum, "Electromagnetic wave propagation along a ferrite loaded wire," *IEEE Trans. Microwave Theory Tech.*, vol. MTT-17, pp. 92–100, Feb. 1969.

[11] D. Polder, "On the theory of ferromagnetic resonance," *Phil. Mag.*, vol. 40, pp. 99–115, Jan. 1949.

[12] K. Whiting, "Design data for UHF circulators," *IEEE Trans. Microwave Theory Tech.* (Corresp.), vol. MTT-15, pp. 195–198, Mar 1968.